

Halo Occupation Distribution estimation performance for LSST data

P. Cataldi¹, V. Cristiani^{2,3,4}, F. Rodriguez^{2,3,4}, A. Taverna^{2,5,6}, M.C. Artale⁷, B. Levine⁸ & the LSST Dark Energy Science Collaboration

¹ Instituto de Astronomía y Física del Espacio, CONICET-UBA, Casilla de Correos 67, Suc. 28, 1428, Buenos Aires, Argentina e-mail: pcataldi@iafe.uba.ar

² Instituto de Astronomía Teórica y Experimental - Observatorio Astronómico de Córdoba (IATE, UNC-CONICET), Córdoba, Argentina

³ Observatorio Astronómico de Córdoba, Universidad Nacional de Córdoba, Laprida 854, X5000BGR, Córdoba, Argentina

⁴ Facultad de Matemática, Astronomía y Física, Universidad Nacional de Córdoba (FaMAF-UNC). Bvd. Medina Allende s/n, Ciudad Universitaria, X5000HUA, Córdoba, Argentina

⁵ Instituto de Astronomía, Universidad Nacional Autónoma de México, Apdo. Postal 106, Ensenada 22800, B.C., México

⁶ Center for Theoretical Physics, Polish Academy of Sciences, Al. Lotników 32/46, 02-668 Warsaw, Poland

⁷ Universidad Andrés Bello, Facultad de Ciencias Exactas, Departamento de Física y Astronomía, Instituto de Astrofísica, Fernández Concha 700, Las Condes, Santiago RM, Chile

⁸ Department of Physics and Astronomy, Stony Brook University, Stony Brook, NY 11794, USA

Received XX, XXXX; accepted XX, XXXX

ABSTRACT

Context. Upcoming imaging surveys, such as the Vera C. Rubin Observatory Legacy Survey of Space and Time (LSST), will enable high signal-to-noise measurements of galaxy clustering. The halo occupation distribution (HOD) is a widely used framework to describe the connection between galaxies and dark matter haloes, playing a key role in evaluating models of galaxy formation and constraining cosmological parameters. Consequently, developing robust methods for estimating this statistic is crucial to fully exploit data from current and future galaxy surveys.

Aims. The main goal of this project is to extend a background subtraction method to estimate the HOD with more photometry-based information in preparation for the clustering analysis of the upcoming LSST data and to enable the study of the HOD with significantly improved statistical power. We evaluate the performance of the method using a mock galaxy redshift survey constructed from the COSMOC2 catalogue.

Methods. We implement an extension of the background subtraction technique to utilize information from photometric galaxy surveys. To identify the centres of galaxy groups, we implement an iterative centroiding approach (Central Galaxy Finder). We evaluate the impact of each step in our pipeline, including group size estimation from luminosity and *purity*, and *completeness* on group identification, along with the influence of observational systematics such as the use of photometric redshifts and halo mass uncertainties.

Results. We demonstrate the validity of the proposed method using a mock galaxy catalogue, recovering the HOD from COSMOC2 over the absolute magnitude range $M_r = -20.0$ to -17.0 and halo masses up to $10^{15} M_\odot$. We present key performance metrics to quantify the precision and reliability of the group finder and the resulting HOD measurements.

Key words. dark matter – galaxies: halos – large-scale structure of universe – methods: statistical

1. Introduction

Understanding how galaxies trace the underlying dark matter distribution is a central goal of modern astrophysics. In the Λ Cold Dark Matter (Λ CDM) paradigm, galaxies form within the gravitational potential wells of dark matter haloes where structure formation is hierarchical: smaller haloes collapse first and subsequently merge to build larger systems (White & Rees 1978). However, the diversity and complexity of the astrophysical processes involved in galaxy formation and evolution pose significant challenges in determining exactly how galaxies occupy and populate dark matter haloes.

The link between galaxies and haloes is fundamental for several reasons. First, it provides a way to infer cosmological constraints. Galaxy surveys allow us to study the spatial distribution of haloes through measures such as galaxy clustering, and infer key cosmological parameters (van den Bosch et al. 2003; Zheng et al. 2005). Furthermore, it provides a framework to explain the physics behind galaxy formation, allowing the contribution of central and satellite galaxies to be studied separately (Kravtsov et al. 2004; Cooray 2005; White et al. 2007; Yang et al. 2008). Observationally, central galaxies are identified as those located near the centres of galaxy groups or clusters, or as galaxies lacking comparably bright neighbours. Theoretically, they are expected to reside close to the minimum of the gravita-

tional potential of their host dark matter haloes. Satellite galaxies correspond to the remaining group members.

Two commonly used statistical approaches to describe the galaxy–halo connection are the Conditional Luminosity Function (CLF) and the Halo Occupation Distribution (HOD). The CLF (e.g. van den Bosch et al. 2003; Yang et al. 2005; van den Bosch et al. 2007) describes the average number of galaxies with luminosity $L \pm dL/2$ that reside in haloes of mass M_h . The HOD (e.g. Jing et al. 1998; Peacock & Smith 2000; Zheng et al. 2005; Tinker et al. 2005) defines the probability distribution $P(N|M_h)$, representing the likelihood that a halo of mass M_h hosts N galaxies with certain properties, typically distinguishing between central and satellite populations. While both approaches are closely related, the CLF is typically framed in terms of luminosity, whereas the HOD focuses on galaxy number counts.

The development of HOD models in the early 2000s (e.g. Seljak 2000; Wechsler et al. 2001; Scoccimarro et al. 2001; Berlind & Weinberg 2002) represented a major advance in linking galaxy clustering with halo statistics. These models have since been used to constrain both galaxy formation scenarios and cosmological parameters. Later studies have refined and applied the HOD formalism across a wide range of galaxy samples (e.g. Mandelbaum et al. 2006; Brown et al. 2008; Agustsson & Brainerd 2006; More et al. 2009; Cacciato et al. 2009; Neistein et al. 2011; Avila-Reese et al. 2011; Leauthaud et al. 2012), confirming its effectiveness in connecting observed galaxies to the underlying dark matter structure. The HOD of dark matter haloes typically follows a simple form: satellite occupation scales with halo mass via a power-law relation ($N \propto M_h^\alpha$), and each halo typically hosts a central galaxy (Kravtsov et al. 2004).

A key challenge in studying satellite galaxies is the limited availability of spectroscopic data. Any satellite-counting exercise is complicated by the faintness of the satellites, which makes obtaining redshift information difficult. To address this, Liu et al. (2011) proposed a method based on photometric data to identify candidate satellites surrounding central galaxies, followed by statistical corrections for foreground and background contamination. This approach can be further improved using a background subtraction technique (hereafter BST), which is effective for analysing galaxy populations statistically (Lares et al. 2011). Several studies, from early works (Holmberg 1969; Phillipps & Shanks 1987) to more recent efforts (Rodriguez et al. 2015; Duckworth et al. 2019), have demonstrated the value of combining spectroscopic and photometric surveys to detect satellite galaxies at fainter magnitudes.

Rodriguez et al. (2015) validated the BST for estimating HODs using mock catalogues constructed from semi-analytic galaxy formation models within the Millennium simulation (Springel et al. 2005). They found a strong overall agreement between the HODs obtained via BST and those derived from direct galaxy counts in volume-limited samples across different absolute magnitude thresholds. Despite a slight overestimation at the faint end ($M_{\text{lim}} \approx -16.0$), the method was shown to be reliable across the full magnitude range ($-21.5 < M_r < -17.0$) (see Fig. 1 in Rodriguez et al. 2015).

In this work, we seek to extend the BST for estimating the HOD using galaxy catalogues primarily based on photometric data. Unlike previous implementations, such as Rodriguez et al. (2015), which relied on spectroscopically confirmed group positions and masses, our method requires a

catalogue for estimating total group masses, but uses angular positions and apparent magnitudes for the rest. This approach reduces the reliance on spectroscopic observations, enabling the inclusion of much larger and deeper samples. In particular, it facilitates the study of more distant galaxy groups and broadens the accessible mass range of the resulting group samples.

Successfully adapting BST to photometric data would make it applicable to current and forthcoming wide-field surveys such as the Vera C. Rubin Observatory Legacy Survey of Space and Time (LSST; LSST Science Collaboration et al. 2009; LSST Dark Energy Science Collaboration 2012), Roman (Spergel et al. 2015; Akeson et al. 2019), and Euclid (Laureijs et al. 2011). These surveys will deliver unprecedented sky coverage, depth, and galaxy number densities—LSST alone will observe billions of galaxies out to $z \sim 3$ and identify around 100,000 galaxy clusters up to $z \sim 1$. A BST optimised for photometric data would therefore provide a timely and powerful tool to exploit these datasets, significantly enhancing the statistical power of HOD studies.

This paper is structured as follows. In Sect. 2 we present the mock catalogue and the object sample used in this work. Sect. 3 and Sect. 4 describe the background subtraction and central galaxy identification techniques. Sect. 5 outlines our testing of the method and details the methods applied for halo mass assignment, and photometric redshift estimation. Finally, we summarise our conclusions in Sect. 6.

2. Data

This work is based on the Data Challenge 2 (DC2) dataset (Korytov et al. 2019; Kovacs et al. 2022) developed by the LSST Dark Energy Science Collaboration (LSST Dark Energy Science Collaboration (LSST DESC) et al. 2021), which covers 440 deg² and is designed for testing and developing LSST analysis pipelines. The core of DC2 is the COSMOSDC2 galaxy catalogue, built from the Outer Rim N-body simulation (Heitmann et al. 2019). Dark matter haloes were identified using a friends-of-friends (FoF) algorithm (Davis et al. 1985) (linking length of $b = 0.168$), with two mass definitions provided: the total FoF mass M_{FoF} and the spherical overdensity (SO) mass M_{200} . The SO of the haloes is defined as the mass within a sphere of radius (r_{200}), whose mean internal density is 200 times the critical density of the Universe at redshift z .

Galaxies were populated using UniverseMachine (Behroozi et al. 2019) and GalSampler (Hearin et al. 2020), with their physical and photometric properties generated through the Galacticus semi-analytic model (Benson 2010). Spectral energy distributions (SED) were built from stellar population models using FSPS (Conroy 2013). The final catalogue includes approximately 2.26 billion galaxies, each with ~ 550 properties—such as stellar mass, morphology, magnitudes in six LSST bands, redshift, and lensing quantities. The simulation assumes an idealised setting, free of dust extinction or stellar contamination. Although stellar masses are taken directly from the simulation and do not enter the BST—contributing only indirectly to the validation tests—luminosities are used to estimate the group radius, as described in Subsection 5.2. These luminosities are computed in the observer frame by blue-shifting the filter transmission functions according to the cosmological redshift (with peculiar velocities

neglected), while k -corrections are interpolated to the lightcone redshifts to minimise discreteness effects in the observed colour space.

To account for photometric redshift uncertainties, we use the COSMOC2 photo- z add-on catalogues produced by DESC: FlexZBoost (Izbicki & Lee 2017) and BPZ (Bayesian Photometric Redshifts; Benítez 2011). FlexZBoost is based on an empirical machine learning method that estimates conditional redshift distributions $P(z|m)$ from photometry in the LSST bands. BPZ is a template-fitting approach that incorporates SED models and galaxy-type priors. FlexZBoost and BPZ have demonstrated high accuracy in previous studies (e.g.; Schmidt et al. 2020; Payerne et al. 2025) and are suited for statistical applications such as HOD estimation.

2.1. Group and galaxy catalogues

Galaxy groups can be identified via their member galaxies using the galaxy catalogues of COSMOC2. Importantly, selecting groups directly from the COSMOC2 galaxy catalogue ensures that the resulting group catalogue remains unaffected by atmospheric or instrumental effects. The COSMOC2 catalogue includes information on galaxy group positions, redshifts, and halo masses.

We construct a mock catalogue using synthetic galaxies extracted from a semi-analytic model of galaxy formation applied to the COSMOC2 simulation. We build this catalogue by collecting a comprehensive set of galaxy properties, including angular positions on the sky (RA, DEC), halo id (HALO_ID), magnitude in the r LSST bands (MAG_R_LSST), stellar and halo masses (STELLAR_MASS, HALO_MASS), and a flag indicating whether each galaxy is central (IS_CENTRAL). We also include the *true* redshift (REDSHIFT), the corresponding photometric redshift estimates from FlexZBoost and BPZ, (PHOTO_Z_MEAN), and the derived redshift quality metric (PHOTO_Z_ODDS). From this full dataset, we select galaxies with a *true* redshift $z < 0.4$ and apparent r -band magnitude $m_r < 21$, resulting in a sample of approximately 1.15×10^6 galaxies. The magnitude cut ensures high completeness, as $m_r < 21$ can be easily achieved with the LSST single-visit depth, while the redshift limit guarantees that we retain all potential satellite galaxies associated with the highest redshift volume-limited sample used in this work ($z_{\max} = 0.304$).

Constructing volume-limited samples is crucial to mitigate redshift-dependent incompleteness resulting from observational limits on apparent magnitude. At higher redshifts, fainter galaxies fall below the detection threshold, making it increasingly difficult to identify low-luminosity systems. This incompleteness can indirectly impact the halo mass range being probed, since lower-mass haloes tend to contain lower-mass, fainter galaxies, which are preferentially lost at higher redshift.

To ensure completeness, we define several absolute magnitude limits, $M_r < -17$, -18 , -19 , and -20 , each corresponding to a higher redshift cut and a brighter selection threshold. For each magnitude cut, we apply a redshift limit to guarantee that the brightest galaxy in each group remains observable across the entire volume. The selection criteria applied to the galaxy catalogue is illustrated in Fig. 1, while the resulting subsample properties—including the number of galaxies, number of central galaxies, and their number densities—are summarised in Tab 1.

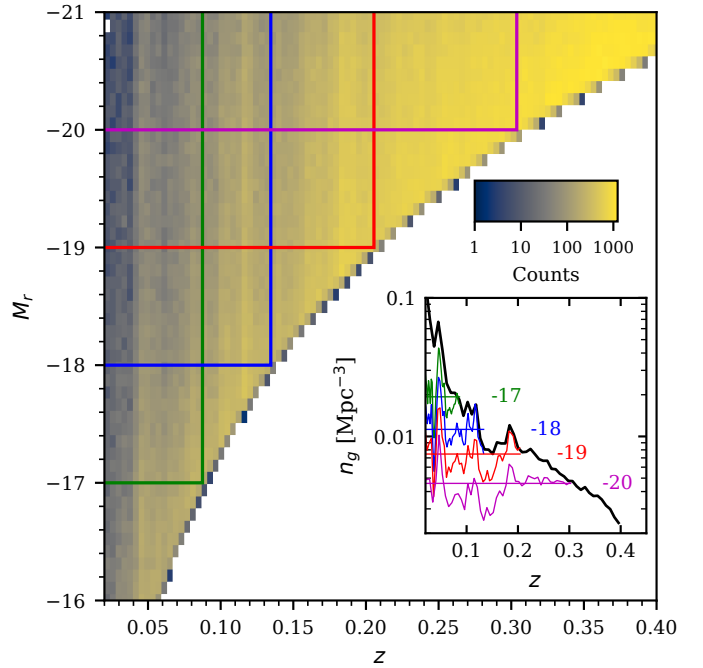


Fig. 1. Construction of volume-limited galaxy samples with varying luminosity thresholds. The colour map shows the distribution of COSMOC2 galaxies as a function of *true* redshift z and r -band absolute magnitude M_r . The different coloured lines delineate the selection boundaries for the volume-limited samples. The *inset panel* shows their mean galaxy number density n_g (colour lines) and total sample density (black line). The solid horizontal lines show the average number density for each sample (the values are given in Tab. 1).

Table 1. Galaxy samples used to test the method described in subsection 5.1. Group centres correspond to central galaxies with absolute magnitudes $M_r < -19.5$. Each row represents a different selection based on magnitude and completeness cuts. The mean galaxy number density n_g is in units of 10^{-3}Mpc^{-3} .

M_{lim}	z_{max}	N_{gal}	N_{cen}	n_g
-17	0.088	$4.1 \cdot 10^4$	$8.8 \cdot 10^3$	19.3
-18	0.135	$8.5 \cdot 10^4$	$2.9 \cdot 10^4$	11.2
-19	0.206	$1.9 \cdot 10^5$	$1.1 \cdot 10^5$	7.5
-20	0.304	$3.5 \cdot 10^5$	$3.2 \cdot 10^5$	4.6

We restrict the luminosity of group members: they must contain at least one bright galaxy to be considered a group. We define a bright galaxy as one with an absolute r -band magnitude $M_r < -19.5$ ¹, following Rodriguez & Merchán (2020) and Zandivarez et al. (2024). Thus, in our analysis, a group of galaxies is a gravitationally bound system that contains at least one bright (central) galaxy. The central galaxies in this magnitude-limited subset are used to define the group centres.

Central and satellite galaxies exhibit different distributions for their properties, as shown in Fig. 2. The black histogram represents all true central galaxies, while the red

¹ This particular choice is motivated by consistency with the methodology adopted in previous works (Yang et al. 2008; Tempel et al. 2009; Rodriguez & Merchán 2020; Yang et al. 2021)

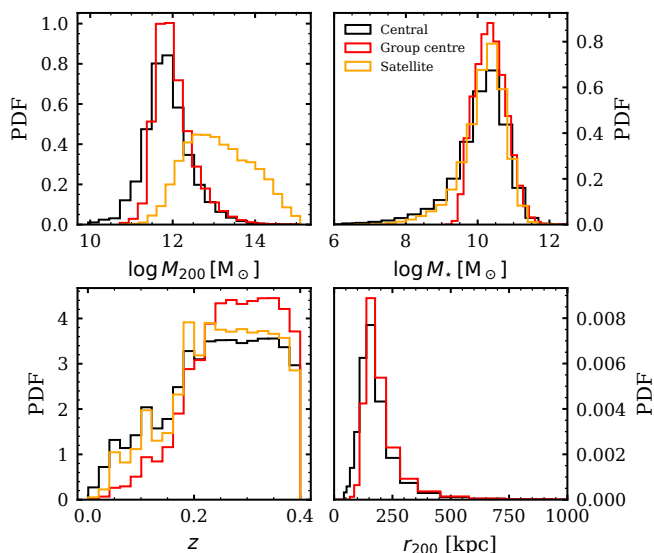


Fig. 2. Normalized distributions for our galaxy catalogue, shown separately for centrals (black), group centres (red), and satellites (orange) galaxies. Panels show the distributions of halo mass M_{200} (top left), stellar mass M_* (top right), galaxy redshift z (bottom left); and halo radius r_{200} , derived from the halo mass (bottom right). The halo radius distribution includes only the central and group centre samples. All distributions are shown for the combined sample used in our analysis, which includes galaxies across the four absolute magnitude cuts.

histogram shows the group centres defined above. Yellow lines indicate satellite galaxies, defined as those not labelled as centrals in the simulation.

As expected, the halo mass distribution for central galaxies presents a peak at a lower mass than that of satellites. This arises from the fact that low-mass haloes tend to have one (central) galaxy, while massive haloes are likely to host satellite galaxies. Both true centrals and our group centres show similar stellar mass peaks; however, the latter tend to be slightly more massive on average. This reflects the fact that their selection is based on brightness, which naturally favours galaxies with higher stellar and halo masses, excluding fainter, low-mass centrals.

In this work, we investigate the impact of photometric redshifts on the performance of the BST at determining group centres. To that end, we use for group centres the photometric redshift add-on COSMOC2 catalogues derived from FlexZBoost and BPZ. Fig. 3 presents a comparison between *true* redshifts (z_{true}) and photometric redshifts (z_{photo}). The dashed lines represent the one-to-one relation, highlighting where photometric redshifts perfectly match the true values. Despite being unbiased, there is a considerable scatter between the photometric and *true* redshifts, with FlexZBoost providing lower dispersion than BPZ. Nevertheless, FlexZBoost results should be considered optimistic due to the deep selection of the training complete sample up to $i < 25$ (and thus unrealistic for real data), while the “discreteness” in the colour-redshift of the modelled galaxies (Korytov et al. 2019) negatively impacts the performance of BPZ. As pointed out in Payerne et al. (2025): the actual LSST data will most likely fall between the pessimistic BPZ and optimistic FlexZBoost runs we analysed.

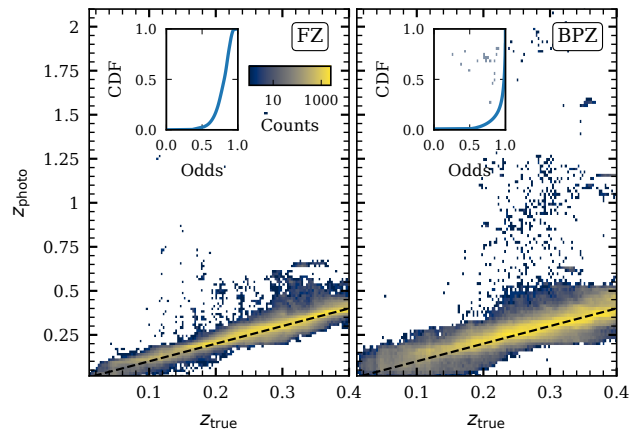


Fig. 3. (Left) Comparison between central galaxies’ *true* redshifts (z_{true}) and photometric redshifts using FlexZBoost (z_{photo} , mean value). (Right) same as left but for BPZ redshifts. The dashed line represents the one-to-one relation ($z_{\text{photo}} = z_{\text{true}}$). The *inset panels* show the cumulative distribution function (CDF) of Odds parameters.

This uncertainty in redshift, and therefore in inferred galaxy positions, significantly complicates the recovery of galaxy clustering signals. Nonetheless, photometric surveys offer the advantage of much larger galaxy samples. Large errors in the photometric redshift are especially common for faint blue galaxies, whose colours can appear similar at both low and high redshifts, making them difficult to distinguish in photometric surveys. The quality-derived redshift PHOTO_Z_ODDS parameter (hereafter, Odds) provides additional insight into the reliability of a photometric redshift estimate (see *inset panels* of Fig. 3). It quantifies how peaked the redshift probability distribution function (PDF) is by integrating the PDF within a defined interval around its mode. A high Odds value indicates a narrow, well-constrained PDF, suggesting that the algorithm is confident in a specific redshift solution. In contrast, a low Odds value implies that the PDF is either broad or multi-modal, reflecting greater uncertainty or the presence of multiple plausible redshift solutions. In the context of this work, we test the performance of photometric redshift estimates and, where appropriate, apply an Odds-based selection to our galaxy catalogue to obtain more constrained subsamples. We note, however, that while an Odds cut can significantly remove a good deal of the outliers, it does not eliminate them entirely and may also remove a substantial number of well-estimated galaxies with point estimates near the true redshifts.

3. Background subtraction technique

The BST has been validated through comparisons with other HOD estimation methods based on observational data. BST can yield results consistent with those obtained from spectroscopically identified galaxy groups, while enabling the study of satellite populations at fainter absolute magnitudes than previously accessible (see Fig. 5 in Rodriguez et al. 2015). The method has been successfully applied in various contexts, including the investigation of the environmental dependence of kinematically misaligned galaxies using MaNGA data (Duckworth et al. 2019), and

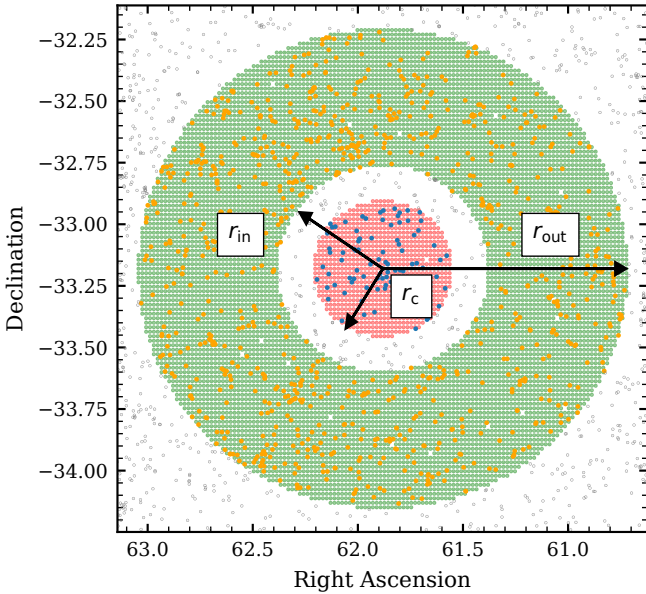


Fig. 4. Illustration of the BST for a single group. The red-shaded area and blue dots indicate the region and galaxies located within the characteristic radius of the host halo ($r < r_c$). The green-shaded area and yellow dots represent the region and galaxies located in the outer annulus ($r_{in} < r < r_{out}$). Gray dots correspond to galaxies that lie outside the region considered by the method.

the study of the mass–richness relation using galaxy catalogues from the Sloan Digital Sky Survey (Gonzalez et al. 2016).

The background subtraction procedure assumes that the large-scale distribution of galaxies is isotropic and homogeneous, and that galaxy groups represent local overdensities. This technique allows estimation of the number of galaxies that appear to belong to a group in projection, but are in fact located in front of or behind it (commonly referred to as background galaxies, although some may lie in the foreground), using statistical analysis. Given the sky area and depth of LSST-like photometric catalogues, by combining spectroscopic surveys for central galaxies with photometric galaxy catalogues, we can estimate the HOD over a wider magnitude range and improve the overall statistics. The primary advantage of this approach is its ability to determine the HOD of satellite galaxies to fainter magnitudes than previously studied.

In Fig. 4, we show the application of BST to a single group extracted from the COSMOC2 simulation. The figure illustrates the circular aperture used to select candidate members, and the surrounding annuli employed to estimate the local background density. To apply the BST, we follow the steps detailed below:

- Redshift assumption: Given that only photometric information is available, we assume that all galaxies are located at the same redshift as the central galaxy of the group, z_{gr} . In this work, we first adopt the true redshift for the group centres, and subsequently extend the analysis to the case where photometric redshifts are used. The absolute magnitude is then computed as:

$$M = m - 25 - 5 \log(d_L(z_{gr})) \quad (1)$$

where $d_L(z_{gr})$ is the luminosity distance in Mpc at z_{gr} .

- Galaxy counting: Define n_i as the number of galaxies with absolute magnitude $M_r < M_{lim}$ within a circle centred in each group with a radius determined by some projected characteristic radius of the halo (r_c), which is often taken to be r_{200} . The value of M_{lim} sets the upper limit for the range of absolute magnitudes where the HOD will be estimated.
- Background estimation: A statistical method is necessary, as the background contribution to n_i is challenging to determine directly. Given the hierarchical nature of large-scale structure, it is known that a given overdensity is always embedded in a larger density mode, which may cause the matter density nearby to be greater or less than the cosmic mean. To estimate the number of background galaxies (n_0), count those that satisfy the same magnitude criterion in an annulus ($r_{in} < r < r_{out}$) around each group, rather than using a global average.
- Background subtraction: To discount the contribution of background galaxies, which cannot be distinguished from the group galaxies, we need to determine their number density in the region surrounding the group. We compute the corrected number of galaxies N in each group using:

$$N = n_i - \frac{n_0}{A_0} A_i \quad (2)$$

where n_0 is the galaxy count in the annulus, and A_i and A_0 are the projected areas of the group circle and background annulus, respectively.

- Sample selection: Since the method has no restrictions on the choice of groups, we should be careful when selecting the samples used in each measurement. Specifically, low-mass groups cannot be detected at high redshifts because they typically contain faint galaxies, while high-mass groups can be observed across the entire redshift range. This is addressed by setting a redshift limit z_{max} for each mass bin, such that the brightest galaxy in each group is detectable.
- HOD estimation: Bin the groups by halo mass and compute the HOD as the average number of galaxies per group: $\langle N|M_h \rangle$, considering only those groups for which galaxies with M_{lim} , located at z_{gr} , would have an apparent magnitude brighter than the limiting apparent magnitude of the photometric catalogue.

3.1. Extension to photometric data

Traditionally, implementing BST requires detailed information for each group, including halo mass, redshift, angular position, and a characteristic radius, alongside a galaxy catalogue containing angular positions and magnitudes.

We adapt this framework to operate solely on photometric catalogues, removing the reliance on spectroscopically confirmed group properties. To achieve this, we incorporate a complementary method to identify potential central galaxies directly from photometric data. This approach is referred to as the *Central Galaxy Finder* (CGF) and is outlined in Sect. 4. We also leverage available photometric redshift estimates to statistically constrain galaxy membership and estimate the HOD.

Our approach is more challenging due to the inherent uncertainty in photometric redshifts, but it enables the application of the method to the full depth and area of upcoming wide-field photometric surveys. Moreover, this implementation lays the groundwork for a wide range of future

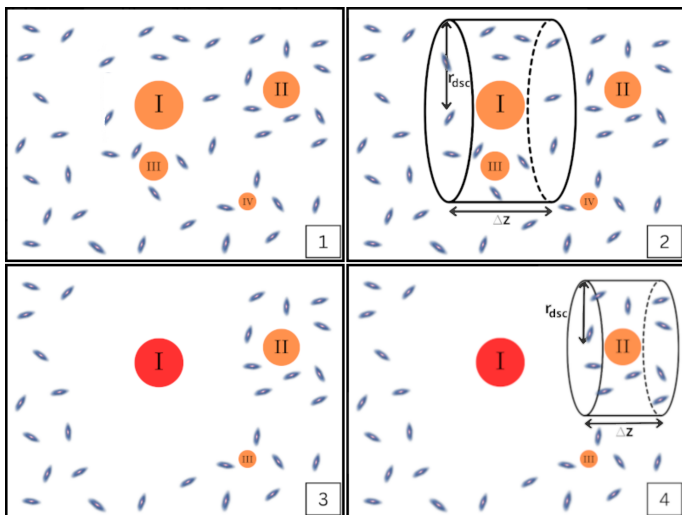


Fig. 5. Scheme of the CGF method applied to a galaxy sample. Top left: selection of candidate group centres, ranked by brightness (orange dots). Top right: definition of a discard region centred on the brightest galaxy (I), determined by its luminosity. Bottom left: removal of all galaxies within the discard region from the candidate list, except for galaxy (I). Bottom right: continue with the next remaining brightest galaxy. In all panels, the line of sight is along the direction perpendicular to the plane of the plot (i.e. viewed from the side of the plot).

studies on the galaxy–halo connection, including halo assembly bias, galactic conformity, and secondary clustering dependence on properties such as colour and environment density.

4. Central Galaxy Finder (CGF)

In this work, we extend the BST algorithm to enable its application to galaxies with only photometric information. To make this extension feasible, it is first necessary to identify potential galaxy groups—or at least their central galaxies—using photometric data alone, since the BST method requires accurate group positions.

In this context, we introduce a method to identify central galaxy candidates based on their brightness relative to the local galaxy density. This step provides the necessary input catalogue of group positions and properties to which the BST can be applied. Alternatively, other group finder algorithms designed to be used in large photometric surveys can also be used in conjunction with the BST, such as redMaPPer (Rykoff et al. 2014), CFSFDP (Zou et al. 2021), and WaZP (Aguena et al. 2021). Below, we outline the main steps employed in our *Central Galaxy Finder* (CGF, see Fig. 5 for a schematic illustration.)

Step 1: Initial Selection. We begin by selecting all galaxies with an absolute magnitude in the r -band of $M_r < -19.5$. These galaxies are considered potential group candidates and are ordered in decreasing luminosity. Step 1 is illustrated in panel 1 of Fig. 5, showing the full sample of luminous galaxies.

Step 2: Discard-radius estimation. Starting with the brightest galaxy in the list, we estimate its discard group radius using the relation $r_{\text{dsc}} = f_r \cdot r_c$, where f_r is a free scaling parameter and r_c is the previously mentioned characteristic radius of the halo. The radius r_{dsc} defines the projected search region for potential group members and is referred to

as the *discard radius*. This projected volume for the brightest galaxy is shown in panel 2 of Fig. 5.

Step 3: Member Selection. We select all galaxies that lie within a projected distance $r < r_{\text{dsc}}$ and have a redshift difference $\Delta z < f_z$, where $\Delta z = |z_{\text{can}} - z_{\text{gal}}|$. Here, z_{can} is the redshift of the brightest galaxy, and z_{gal} is the redshift of the other candidates. The parameter f_z is another free variable of the method. All selected galaxies are marked as members of the group, and they are then removed from the catalogue for subsequent steps. Panel 3 of Fig. 5 shows the catalogue after discarding the identified group members.

Step 4: Iteration. We move to the next brightest galaxy that has not been previously discarded, and repeat Steps 2 and 3. Panel 4 in Fig. 5 illustrates this step, where the selection moves to the next remaining bright galaxy. This iterative process continues until the entire catalogue has been processed.

For reliable HOD estimation, high central galaxy *purity* across the full halo mass range is essential—and also the most challenging to achieve. *Purity* is defined as the percentage of selected candidates that are truly central galaxies, and *completeness* is defined as the fraction of true centrals that are correctly identified.

In Fig. 6, we present the resulting *purity* and *completeness* of the identified central galaxy candidates for a fixed set of parameters: $(f_r, f_z) = (2.5, 0.25)$, shown as a function of absolute magnitude (left panel), stellar mass (middle), and halo mass (right), with different coloured lines indicating median values under various magnitude cuts representing different observational selections. The choices of this fixed set of parameters improve the *purity* of true centrals (above $\sim 70\%$ over halo mass) by excluding interlopers over a larger projected and redshift volume. Although this configuration results in lower *completeness*, this is less concerning for future photometric surveys due to their large statistical samples.

The characteristic U-shaped trend in *purity* across M_r , M_\star , and most prominently M_{200} , arises naturally from the way the CGF operates. Because the CGF initially selects the brightest galaxies in the catalogue, these early candidates are, in the vast majority of cases, *true* centrals. They are also less likely to be removed in the iterative discard steps of the algorithm. This leads to both high *completeness* and high *purity* at the bright/massive end. As the CGF continues through the candidate list, progressively fainter galaxies are examined. At this stage, *completeness* decreases because more galaxies are discarded during iteration, including some genuine centrals. *Purity* also declines because the removal of a *true* central can result in an “orphan” group, for which the CGF assigns the brightest remaining galaxy in the local region—often a satellite. This effect drives the drop in *purity* at intermediate magnitudes, stellar masses, and halo masses.

At the faint/low-mass end, the *completeness* is indeed lower (these galaxies are considered last in the CGF iteration cycle), but most of the corresponding haloes host only one or two members. In such cases, the CGF classification is typically correct, which produces the recovery in *purity* at the faint end. Finally, the more pronounced U-shape observed when *purity* is plotted against M_{200} reflects the fact that the CGF selection is based on brightness (and therefore indirectly on M_\star), so *purity* is expected to be systematically lower and to show stronger variations across halo mass bins.

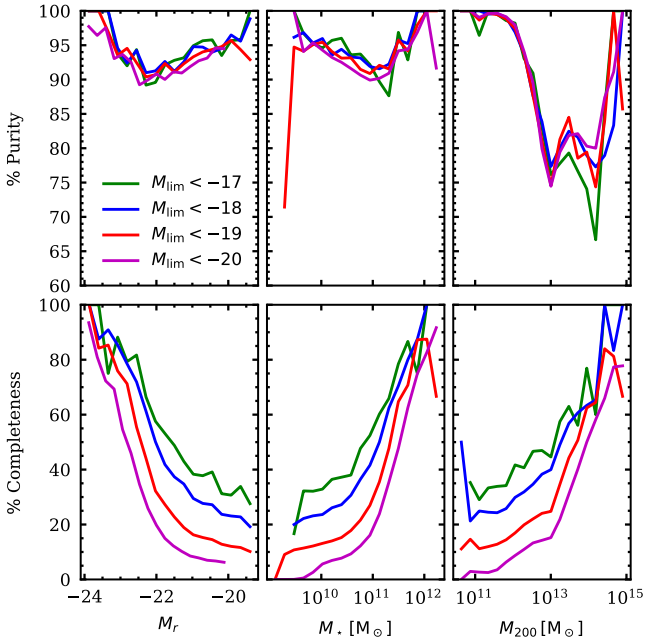


Fig. 6. (Top panels) *Purity* of the resulting catalogue as a function of absolute magnitude (left), stellar mass (middle), and halo mass (right). The galaxies were selected from the CGF method with a fixed $f_r = 2.5$ and a redshift bin width of $f_z = 0.25$. (Bottom panels) Corresponding *completeness* shown as a function of the same variables. Different coloured lines represent the median values for the volume-limited samples.

To further understand the trade-offs involved, Fig. A.1 (Appendix A) presents the *purity* and *completeness* of the CGF as a function of halo mass (M_{200}) in the range 10^{12} – $10^{15} M_{\odot}$, focusing on this high-mass regime where achieving high *purity* for central galaxies is particularly challenging. We find a clear tension between *purity* and *completeness* across different combinations of f_r and f_z : high values of both parameters increase the exclusion volume in each iteration of the CGF, resulting in high *purity* but reduced *completeness*. Conversely, lower values of f_r and f_z improve *completeness* by retaining more candidates, but at the cost of lower *purity* due to increased contamination. Given that future surveys such as LSST will provide excellent statistics through large galaxy samples, we opt for a parameter set that prioritises higher *purity*, ensuring more accurate central galaxy identification and thus more reliable HOD recovery.

The CGF naturally favours isolated, bright galaxies, leading to high purity when selections are based on stellar mass or magnitude. Every group-finding algorithm introduces selection biases arising from the trade-off between purity and completeness. Our CGF-derived central-galaxy catalogue remains broadly consistent with the true centrals from the simulation (see Fig. A.2). For comparison, Yang et al. (2021) reported $\geq 80\%$ completeness in member detection but only $\geq 70\%$ of groups reaching high purity, and their method is reliable only for haloes above $10^{12.5} M_{\odot}$. Likewise, REDMAPPER achieves an almost unbiased cluster catalogue but operates at even higher masses ($M \geq 10^{14} M_{\odot}$), well above the regime relevant for our HOD analysis, where lower-mass systems are more prone to misclassification and mass overestimation.

5. Results

In the following sections, we present a step-by-step evaluation of our method. In Subsection 5.1, we validate the BST using simulation-based quantities such as *true* redshifts, angular positions, halo masses, and central galaxy identifiers to define group centres. Subsection 5.2 explores an alternative approach to estimating group sizes by substituting halo size with luminosity derived from absolute r -band magnitudes. In Subsection 5.3, we investigate the impact of FlexZBoost and BPZ photometric redshifts on the inference of the HOD. Subsection 5.4 assesses the impact of uncertainties in halo mass estimation. Finally, in Subsection 5.5, we evaluate the performance of our method on the CGF outputs applied to photometric data.

5.1. Evaluation of the Method

This section aims to evaluate the performance of BST. To this end, we use the mock catalogue introduced earlier, which provides full knowledge of galaxy populations within dark matter haloes, enabling a direct comparison between the true group properties and those recovered by our method.

As a first test, we apply the technique under idealised conditions: using the true angular positions, redshifts, and halo masses of central galaxies to define group locations, along with the true angular positions of satellite galaxies. This setup isolates the intrinsic accuracy of the method prior to introducing observational uncertainties.

We adopt a characteristic radius of $r_c = r_{200}$, as it serves as a good upper limit for group sizes, defined as the maximum Cartesian distance between the central galaxy and its most distant satellite. The COSMOC2 intra-halo distribution of satellites follows a truncated NFW profile (Korytov et al. 2019), so it is expected that the satellites population drops sharply after $r > r_{200}$.

We impose a maximum radius of $r_c = 1$ Mpc to avoid excessively broad annuli. This ensures that the computed local galaxy density is not diluted by including regions representative of the cosmic mean density, which would otherwise lead to an overestimation of group membership in massive clusters. Only a small fraction of groups exceed this upper limit: about 0.2% for $M_{\text{lim}} = -17$, and even lower fractions for the brighter samples. Therefore, this cut-off has a minimal impact on the overall catalogue.

To compute the background contribution as described in Sect. 3, we define an annular region of $1.5 r_c < r < 3.5 r_c$. We tested different combinations of inner and outer radii of the annular region, specifically $r_{\text{in}} = \{1.5, 2.0, 2.5\}$ and $r_{\text{out}} = \{3.5, 4.0, 4.5, 5.0\}$, and found that the BST results remain stable across all choices, as long as the annular region avoids including actual group members, but is not so large that it samples environments unrepresentative of the local density in the vicinity of the group.

Figure 7 shows the HOD across a broad range of halo masses. The true HOD is computed from the known galaxy group memberships in the mock catalogue by binning in halo mass and averaging the number of galaxies per bin. The black lines represent the median true HOD. The background colour maps display the two-dimensional distribution of galaxy counts recovered using the BST, while the coloured lines show the median HOD for different galaxy samples defined by varying magnitude limits. Uncertainties

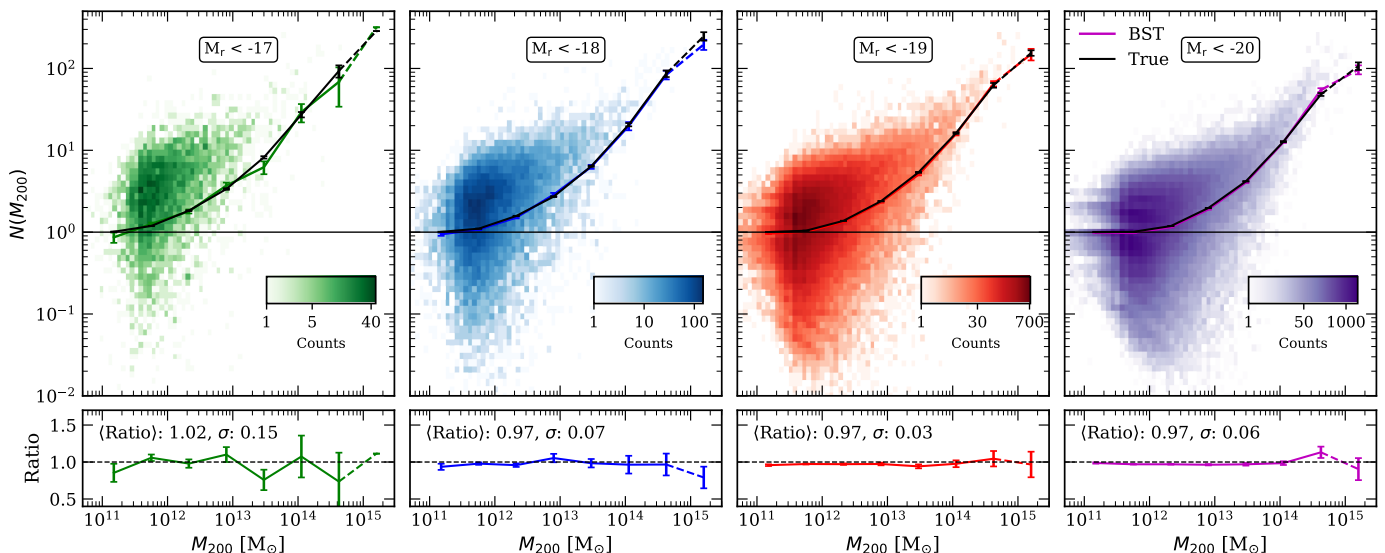


Fig. 7. Comparison between BST results (colour lines) and the *true* HOD obtained by direct counts in volume-limited samples (black lines). Each panel shows results for $M_{\text{lim}} = -17, -18, -19$ and -20 . The colour maps represent the occupation number obtained for each volume-limited sample according to the BST, while the coloured lines indicate the median values of the corresponding distributions. Dashed lines correspond to the highest halo-mass bins ($M_{200} > 5 \times 10^{14} M_{\odot}$), which are affected by low-number statistics. For a better quantification of the differences, the lower panels show the ratio between the BST-recovered and true HOD, where we show the median and dispersion values. All uncertainties were calculated by the standard jackknife procedure.

were estimated using a random jackknife sample, in which the BST output is randomly divided into 50 equal subsets and the HOD is recomputed while omitting each subset in turn. The lower panels show the ratio between the BST and the true HOD, for which we compute the median and dispersion as a quantitative measure of the BST performance.

We find that the agreement between the BST-recovered and true HOD generally improves as the magnitude limit becomes brighter (i.e., lower M_{lim}), which increases the effective redshift range (up to $z < 0.3$) and enhances sample completeness. This improvement is also due to the increased sample size in these brightness bins (see Tab. 1), leading to lower statistical scatter. We note that the median and dispersion of the ratio between the BST-recovered and true HOD are typically below unity; however, in all cases, they remain consistent with unity within the quoted uncertainties. Across the halo mass range, we observe both underestimation and overestimation of the HOD, indicating no systematic bias of the BST-recovered HOD. The offset between the median and the mode of the BST distribution arises from the way the BST computes the number of galaxies in each group through Eq. 2, which can yield $N(M_{200}) \leq 0$ for some groups, particularly at low-density environments. In Fig. 7 we display the results in logarithmic scale, excluding these non-positive values. Nevertheless, all $N(M_{200})$ are included when computing the median relation shown in the HOD analysis.

The highest halo mass bins ($M_{200} > 5 \times 10^{14} M_{\odot}$), indicated with a dashed line, suffer from poor statistics due to the limited number of massive groups in the COSMOC2 simulation. Consequently, the median values in this regime should be interpreted with caution. We include these results for completeness, noting their statistical limitations, and because the recovered HOD still shows reasonable agreement. This issue is expected to be significantly alleviated with future datasets from wide-area surveys such as LSST,

which will cover $\sim 18,000 \text{ deg}^2$ and provide a vastly larger sample of both galaxies and massive clusters

Interestingly, the mock catalogue itself exhibits a flattening of the HOD at the high-mass end, with the number of satellites not increasing as expected. This deviates from the typical HOD behaviour, where the satellite population continues to grow with halo mass, following a power-law slope. Notably, the BST-recovered HOD reproduces this same trend, demonstrating its ability to capture the underlying distribution even in regimes affected by modelling.

5.2. Luminosity-based group size

Reliable determination of group sizes in flux-limited samples is challenging because the number of detected members decreases with distance, introducing strong selection effects (Yang et al. 2008). We aim to estimate the characteristic radius of the host halo used in BST from the observed luminosity of the central galaxy of the group (r_c^{lum}), to avoid relying on parameters from the simulation which we would not have access to in real data.

We compute the linear fit between host halo characteristic radius (r_c) and luminosity for central galaxies, as shown in the left panel of Fig. 8. This relation enables an interpolation scheme to infer r_c , serving as a proxy for group size, directly from the total luminosity of a system. This approach is particularly useful when only photometric data are available.

We propose the relation

$$r_c^{\text{lum}} = C_1 \cdot L + C_2 \quad (3)$$

where $C_1 = 6.1 \times 10^{-10} \text{ Mpc}/L_{\odot}$ and $C_2 = -0.03, \text{ Mpc}$. We show the comparison of r_c^{lum} with r_c in the right panel of Fig. 8. Although both characteristic halo radii can be approximately related through a linear relation, the compar-

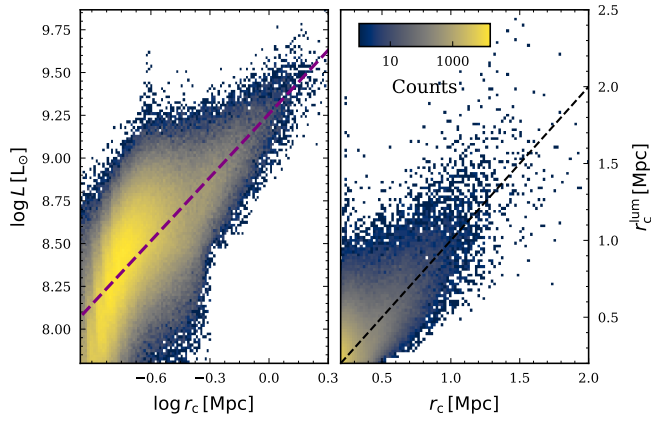


Fig. 8. (Left panel) Relation between r_c and luminosity for central galaxies in our catalogue, with the best linear fit shown as purple dashed lines. (Right panel) Relation between r_c and the estimated r_c^{lum} , with the dashed line indicating the one-to-one relation.

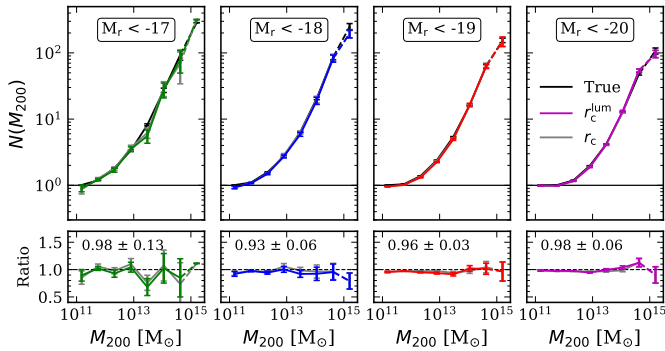


Fig. 9. BST results using r_c^{lum} derived from the central galaxy luminosity using Eq. 3. In gray lines, recovered HOD when using r_c and in black lines, the true HOD. The lower panels show the ratio between the BST-recovered and true HOD, together with the corresponding median and dispersion.

ison reveals a significant dispersion which is expected to impact the HOD estimation.

The results when using r_c^{lum} instead of r_c show good agreement between the recovered HOD and the true HOD across the full halo mass range, presented in Fig. 9. While adopting a more flexible relation between central galaxy luminosity and size—such as a broken power law or a mass-dependent slope—could potentially yield even better results, our current linear parametrisation proves sufficiently accurate and robust for this analysis. This simple model is particularly valuable given the challenge of estimating the group radius, which typically requires a prior determination of its halo mass. In contrast, our approach allows a practical and effective estimation of group size directly from the luminosity of the central galaxy, enabling a reliable recovery of the HOD without detailed mass modelling. In the following sections, we therefore adopt r_c^{lum} , computed from the luminosity of the central galaxies, for the validation of the method.

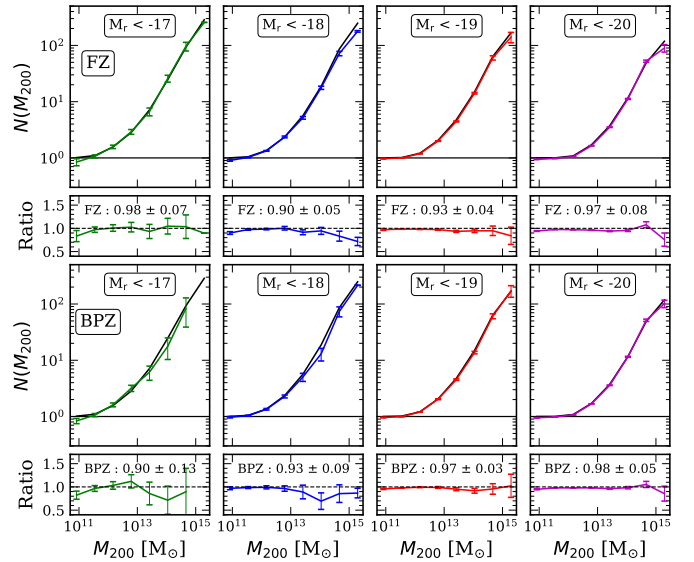


Fig. 10. (Top panels) Recovered BST HODs using FlexZBoost (FZ) photometric redshifts. The black lines show the true HOD. The lower panels show the ratio between the BST-recovered and true HOD, together with the corresponding median and dispersion. (Bottom panels) same as top but for BPZ.

5.3. Photometric redshift

In this subsection, we investigate the impact of using photometric redshifts by adopting redshift estimates from FlexZBoost and BPZ. Specifically, we replace the *true* redshift from the group centres, z_{gr} , with the photometric redshift, z_{photo} , and for estimating r_c^{lum} in BST through Eq. 1. This substitution introduces uncertainty in the absolute magnitude of central galaxies and their associated groups, significantly complicating the recovery of the HOD. Moreover, some migration of galaxies between the volume-limited subsamples is expected once photometric redshifts are applied, as will occur in real observational data.

In this test, we do not apply any quality cut on the photometric redshifts, allowing us to test the robustness of the BST with respect to photometric redshift in the “worst” case scenario—i.e., with no mitigation of the impact of outliers on the final results. The resulting HODs obtained using the BST under these conditions are presented in Fig. 10. Both photometric redshift estimators are generally in good agreement with the truth across all magnitude cuts. BPZ yields lower performance than FlexZBoost, especially in the faintest cut ($M_{\text{lim}} = -17$), due to more dispersed and biased photometric redshifts with respect to the true redshifts.

Uncertainties in the photometric redshifts of group centres do not contribute significantly to the background subtraction estimation of the total HOD. We note that, as shown in Fig. 10, the HOD inferred for groups identified using photometric redshifts exhibits only a mild underestimation at the high-mass end, while otherwise accurately reproducing the true HOD.

5.4. Halo mass estimation

In photometric galaxy surveys, estimating halo masses is inherently challenging due to projection and miscentering effects, limited group membership, and uncertainties in

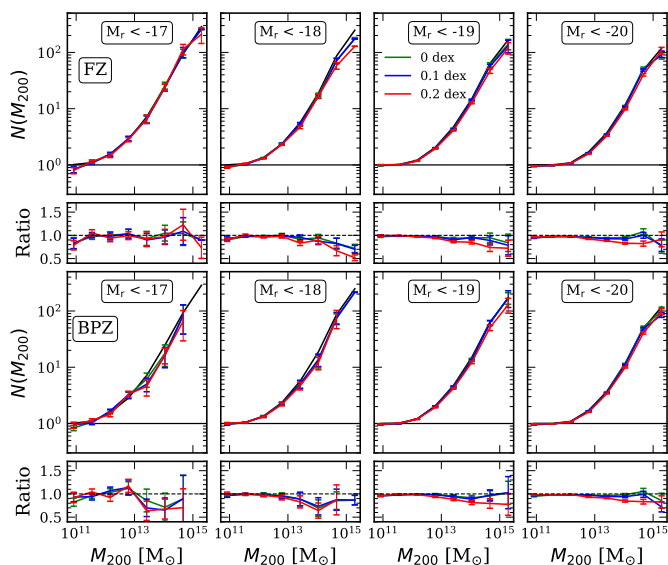


Fig. 11. (Top panels) Recovered HODs using the BST under varying levels of Gaussian uncertainty added to the halo masses, expressed in dex units for FlexZBoost photometric redshifts. (Bottom panels) same as top but for BPZ. Increasing the scatter predominantly affects the high-mass end of the HOD, while the low-mass regime remains largely stable.

galaxy properties. For instance, Yang et al. (2021) obtained halo mass estimates for each group by applying an abundance matching method using total group luminosity ranking, which links stellar mass to halo mass based on cumulative number density matching (e.g.; Moster et al. 2018; Behroozi et al. 2019). Although this empirical approach provides a physically motivated alternative to group-based dynamical mass estimators, accurate stellar masses, star-formation rates, and luminosities are required to obtain reliable halo mass estimates, typically with a mean scatter of $\sigma \sim 0.20$ dex (Van Kampen et al. 2025).

Relying solely on apparent magnitudes of central-galaxy candidates (without confirmed group membership) substantially increases the uncertainties, making it challenging to robustly recover the HOD. An additional source of error arises from redshift uncertainties inherent in the use of photometric catalogues. To assess how such uncertainties might impact our method, we performed a controlled test in which we added a Gaussian dispersion of 0.1 and 0.2 dex to the simulated halo masses. These values reflect the typical maximum scatter observed in the empirical relation between the halo mass and the number of group members. Fig. B.1 (Appendix B) shows the resulting redistribution of halo masses produced by these uncertainties. The associated uncertainty is largest at the low- and high-mass ends, and decreases towards the intermediate mass range.

Figure 11 presents the results of these tests. As shown, the added halo mass uncertainties do not produce a large impact on the recovered HOD, although small deviations become apparent at the high-mass end for the largest mass perturbation considered. BPZ performance weakens, particularly for the fainter magnitude cuts. The overall good agreement between the HODs obtained under different levels of halo mass scatter indicates that the method is robust against typical observational errors in halo mass estimation.

Table 2. Central galaxies identified with the set parameters $(f_r, f_z) = (2.5, 0.25)$ from the CGF method. Each column represents a different selection based on magnitude limits and *completeness* cuts. We also show identified central galaxies with Odds > 0.8 .

M_{lim}	z_{max}	$N_{\text{cen}}^{\text{CGF}}$	$N_{\text{cen}}^{\text{Odds}}$
-17	0.088	$2.9 \cdot 10^3$	$2.3 \cdot 10^3$
-18	0.135	$6.8 \cdot 10^3$	$5.8 \cdot 10^3$
-19	0.206	$1.3 \cdot 10^4$	$1.2 \cdot 10^4$
-20	0.304	$2.0 \cdot 10^4$	$1.9 \cdot 10^4$

5.5. Application of the CGF

In this final subsection, we incorporate the CGF technique into the previously BST recovered HOD to evaluate the impact of group-centre misidentification in combination with all systematic effects considered so far (luminosity-based group size, photometric redshift errors, and a halo mass uncertainty of 0.1 dex). We use CGF fixed parameters $(f_r, f_z) = (2.5, 0.25)$, motivated by previous analysis (see Sect. 4). Consequently, the total number of galaxies identified as central decreases significantly, primarily due to the lower *completeness* associated with these conservative selection parameters. This reduction is quantified in Tab. 2, where the decrease in the number of selected central reflects the trade-off between *completeness* and *purity*. Nonetheless, the gain in *purity* justifies this choice, as it enables a more reliable reconstruction of the true HOD.

In Fig. 12, we present the results of applying the BST to this refined sample of central galaxies. We further restricted to objects with Odds > 0.8 , to reduce the contribution of photometric redshift outliers while preserving a high fraction of the original CGF-identified central galaxies. The HOD recovery shows good agreement with the true underlying distribution for the brighter magnitude limits ($M_{\text{lim}} = -19, -20$). However, performance degrades for the other subsamples, which can be attributed to the low number of galaxies in this subsample (fewer than 10^4). Due to reduced statistics from CGF application, achieving good agreement at the faint end remains challenging for FlexZBoost and BPZ, but both perform well in the brighter cuts. Larger simulations with broader sky coverage—such as a potential extension of SKYSIM5000—would provide improved sampling and enable more robust constraints on the HOD in this regime. Additionally, we note that more sophisticated group-centre identification techniques may yield further improvements; however, the approach adopted here provides satisfactory performance while maintaining a relatively simple methodology.

We further investigate the impact of varying the CGF parameters, f_r and f_z , within the BST framework. Fig. A.3 (Appendix A) shows the effect of changing these parameters on the recovered HOD. We find that increasing f_r leads to better agreement between the recovered and true HOD, primarily through an improvement in the *purity* of central galaxy identification. This effect is particularly relevant at high halo masses, where contamination from misidentified centrals can strongly bias the HOD estimate. In contrast, variations in the redshift discard parameter f_z have a comparatively minor impact on the BST results, indicating that

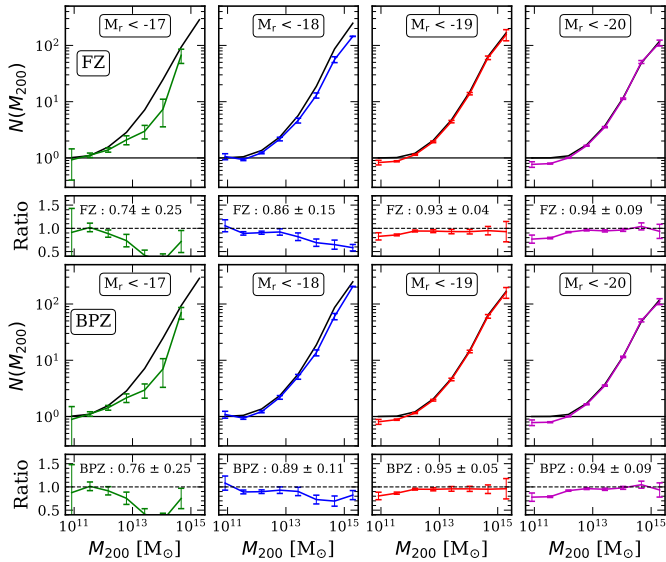


Fig. 12. (Top panels) Results of the BST applied to galaxies identified with the CGF, with parameters $(f_r, f_z) = (2.5, 0.25)$ for FlexZBoost photometric redshifts. The black lines show the true HOD. (Bottom panels) same as top but for BPZ.

the method is less sensitive to this parameter within the explored range.

6. Conclusions

In this paper, we extend the Background Subtraction Technique (BST) developed by Rodriguez et al. (2015) to enable its application to galaxy samples based on both true and photometric redshifts. By incrementally introducing observational uncertainties into the variables involved in BST, we evaluated the ability of the method to recover the Halo Occupation Distribution (HOD). The main modifications and improvements to the original BST are summarised as follows:

- We first evaluated the method by applying BST to the true values of redshift, halo mass, and radii in COSMOC2 and successfully recovered the HOD with excellent agreement. Following the classical BST approach, we used the true central galaxies as group centres with known positions.
- We then replaced the characteristic radius r_c with a more observationally motivated proxy, using the luminosity of the central galaxy (r_c^{lum}), showing that the luminosity-based scaling provides a sufficiently reliable proxy for group sizes within the context of our analysis.
- Next, we then added uncertainty to the group positions by incorporating photometric redshift errors. Despite a significant loss in statistical power due to the limited sky coverage of the DC2 simulation, we were still able to recover the HOD. When introducing typical uncertainties in the halo mass estimation, the HOD recovery remained robust.
- We substituted the known central galaxies from the simulation with an inferred central-galaxy identification method (Central Galaxy Finder, CGF), based on galaxy luminosity and spatial distributions. We achieved a central-galaxy average *purity* greater than 70 %, with

completeness average over 60 % over the halo mass range studied. This simple method effectively recovers the HOD for the brighter cuts, bringing our approach closer to observational techniques for constraining halo occupation.

Table 3 summarises the BST performance across all tests. We recovered the HOD of the COSMOC2 catalogue in four ranges of limiting absolute magnitudes which extend from -17 to -20 in LSST r-band and halo masses up to $10^{15} M_\odot$.

These results demonstrate that the BST can be effectively extended to a broad range of observational datasets, including those with mixed redshift quality and limited group information. Our updated implementation reduces model dependence by relying on observable-based proxies and inference techniques, rather than requiring full spectroscopic group catalogues. This makes the method particularly well-suited for application to deep, wide-field photometric surveys such as LSST, Euclid, and Roman, which will lack complete spectroscopic coverage but offer unprecedented galaxy statistics.

This analysis is still far from the constraining power of an LSST-like survey: the increase in total area from 440 to $18,000 \text{ deg}^2$ corresponds to an enhancement of the galaxy sample by a factor of ~ 41 , and therefore to an improvement of $\sim \sqrt{41}$ in the statistical constraining power of HOD-based analyses. We note, however, that the galaxy samples used in this work are drawn directly from the COSMOC2 simulation, which represents an idealised dataset unaffected by atmospheric or instrumental effects. Although this work provides a thorough rundown of the major systematics relevant to our methodology, stars and blending are not modelled in COSMOC2; nonetheless, our magnitude range ($m_r < 21$) lies well above the regime where blending significantly affects the detection of ultra-faint galaxies. The catalogue also does not include extinction from Milky Way dust or stellar foregrounds, modelling only the reddening due to dust within the host galaxies.

Importantly, the ability to recover the HOD from more photometry-based data opens the door to a wide range of science applications beyond traditional clustering analyses. By enabling the measurement of satellite occupation as a function of secondary galaxy properties—such as colour, local density, star formation rate, and morphology—this approach can contribute to constraining assembly bias and understanding the connection between galaxy evolution and environment. Furthermore, it provides a valuable framework for investigating phenomena such as galactic conformity, where the properties of satellite galaxies correlate with those of their central galaxy. We plan to explore these aspects further with the upcoming LSST data. Importantly, the present work also helps pave the way for the development of cluster-based analyses by providing a pipeline that is readily adaptable to LSST data releases.

Acknowledgements. PC wrote most of the manuscript and created and co-designed all figures, with guidance and input from the co-authors. VC developed most of the CGF method and provided feedback on the results and the manuscript. FR supervised the lead author and contributed to conceptualisation, methodology, project administration, resources, validation, and writing. AT developed the initial data selection, advised on project progress and presentation, and edited the manuscript. MCA edited the manuscript, provided substantial comments and suggestions during the writing process, contributed to the organisation of the paper, and advised on the presentation of the results. BL provided feedback as internal reviewer,

Table 3. Summary of the BST performance across all tests conducted in this work. Each column lists the characteristic halo radius used (r_c), the method adopted to identify group centres, redshift employed for group centres, and the median ratio between the BST–recovered and true HOD values, $\langle \text{HOD}_{\text{BST}}/\text{HOD}_{\text{true}} \rangle$. We only show results for 0.2 dex uncertainty in halo mass. The final column references the corresponding section where each test is discussed.

	Radius	Group Centres	Redshift	$\langle \text{HOD}_{\text{BST}}/\text{HOD}_{\text{true}} \rangle$				Sect.
				$M_r < -17$	$M_r < -18$	$M_r < -19$	$M_r < -20$	
Simulation-Based (Truth)	r_{200}	True centrals	z_{true}	1.02 ± 0.15	0.97 ± 0.07	0.97 ± 0.03	0.97 ± 0.06	Sect. 5.1
Luminosity-Based	r_c^{lum}	True centrals	z_{true}	0.98 ± 0.13	0.93 ± 0.06	0.96 ± 0.03	0.98 ± 0.06	Sect. 5.2
photo-z (FlexZBoost)	r_c^{lum}	True centrals	z_{photo}	0.98 ± 0.07	0.90 ± 0.05	0.93 ± 0.04	0.97 ± 0.08	Sect. 5.3
photo-z (BPZ)	r_c^{lum}	True centrals	z_{photo}	0.90 ± 0.13	0.93 ± 0.09	0.97 ± 0.03	0.98 ± 0.05	Sect. 5.3
Error Mass (FlexZBoost)	r_c^{lum}	True centrals	z_{photo}	0.93 ± 0.11	0.93 ± 0.21	0.89 ± 0.19	0.90 ± 0.08	Sect. 5.4
Error Mass (BPZ)	r_c^{lum}	True centrals	z_{photo}	0.93 ± 0.19	0.89 ± 0.19	0.94 ± 0.08	0.92 ± 0.07	Sect. 5.4
CGF (FlexZBoost)	r_c^{lum}	CGF	z_{photo}	0.74 ± 0.25	0.86 ± 0.15	0.93 ± 0.04	0.94 ± 0.09	Sect. 5.5
CGF (BPZ)	r_c^{lum}	CGF	z_{photo}	0.76 ± 0.25	0.89 ± 0.11	0.95 ± 0.05	0.94 ± 0.09	Sect. 5.5

leading to updates to manuscript structure and content. This paper has undergone internal review in the LSST Dark Energy Science Collaboration. We are very grateful to the internal reviewers: Heidi Wu and Benjamin Levine. PC acknowledges partial support from AN-PCyT through grant PICT 2020-00582. MCA acknowledges support from ANID BASAL project FB210003. VC, FR and AT thank the support by Agencia Nacional de Promoción Científica y Tecnológica, the Consejo Nacional de Investigaciones Científicas y Técnicas (CONICET, Argentina) and the Secretaría de Ciencia y Tecnología de la Universidad Nacional de Córdoba (SeCyT-UNC, Argentina). FR acknowledges support from the ICTP through the Junior Associates Programme 2023-2028. AT acknowledges support from the Dirección General de Asuntos del Personal Académico (DGAPA) of UNAM through the postdoctoral fellowship, and acknowledges support from the PAIRS project via the SONATA grant no.2023/51/D/ST9/02919. DESC acknowledges ongoing support from the IN2P3 (France), the STFC (United Kingdom), and the DOE and LSST Discovery Alliance (United States). DESC uses resources of the IN2P3 Computing Center (CC-IN2P3–Lyon/Villeurbanne - France) funded by the Centre National de la Recherche Scientifique; the National Energy Research Scientific Computing Center, a DOE Office of Science User Facility supported under Contract No. DE-AC02-05CH11231; STFC DiRAC HPC Facilities, funded by UK BEIS National E-infrastructure capital grants; and the UK particle physics grid, supported by the GridPP Collaboration. This work was performed in part under DOE Contract DE-AC02-76SF00515. We thank the developers and maintainers of the following software used in this work: NumPy (van der Walt et al. 2011), SciPy (Jones et al. 2001), Matplotlib (Hunter 2007), Astropy (Astropy Collaboration et al. 2013) and Jupyter (Kluyver et al. 2016).

References

Aguena, M., Benoist, C., da Costa, L. N., et al. 2021, MNRAS, 502, 4435
 Agustsson, I. & Brainerd, T. G. 2006, The Astrophysical Journal, 644, L25
 Akeson, R., Armus, L., Bachelet, E., et al. 2019, arXiv e-prints, arXiv:1902.05569
 Avila-Reese, V., Colín, P., González-Samaniego, A., et al. 2011, ApJ, 736, 134
 Behroozi, P., Wechsler, R. H., Hearin, A. P., & Conroy, C. 2019, MNRAS, 488, 3143
 Benítez, N. 2011, BPZ: Bayesian Photometric Redshift Code, Astrophysics Source Code Library, record ascl:1108.011
 Benson, A. 2010, New Astronomy, 17
 Berlind, A. A. & Weinberg, D. H. 2002, ApJ, 575, 587
 Brown, M. J. I., Zheng, Z., White, M., et al. 2008, ApJ, 682, 937
 Cacciato, M., van den Bosch, F. C., More, S., et al. 2009, MNRAS, 394, 929
 Conroy, C. 2013, ARA&A, 51, 393
 Cooray, A. 2005, MNRAS, 364, 303
 Davis, M., Efstathiou, G., Frenk, C. S., & White, S. D. M. 1985, ApJ, 292, 371
 Duckworth, C., Tojeiro, R., Kraljic, K., et al. 2019, MNRAS, 483, 172

Gonzalez, E. J., Rodriguez, F., García Lambas, D., et al. 2016, Monthly Notices of the Royal Astronomical Society, stw2803
 Hearin, A., Korytov, D., Kovacs, E., et al. 2020, MNRAS, 495, 5040
 Heitmann, K., Finkel, H., Pope, A., et al. 2019, ApJS, 245, 16
 Holmberg, E. 1969, Arkiv for Astronomi, 5, 305
 Izbicki, R. & Lee, A. B. 2017, arXiv e-prints, arXiv:1704.08095
 Jing, Y. P., Mo, H. J., & Börner, G. 1998, ApJ, 494, 1
 Korytov, D., Hearin, A., Kovacs, E., et al. 2019, ApJS, 245, 26
 Kovacs, E., Mao, Y.-Y., Aguena, M., et al. 2022, The Open Journal of Astrophysics, 5, 1
 Kravtsov, A. V., Berlind, A. A., Wechsler, R. H., et al. 2004, ApJ, 609, 35
 Lares, M., Lambas, D. G., & Domínguez, M. J. 2011, AJ, 142, 13
 Laureijs, R., Amiaux, J., Arduini, S., et al. 2011, arXiv e-prints, arXiv:1110.3193
 Leauthaud, A., Tinker, J., Bundy, K., et al. 2012, ApJ, 744, 159
 Lederman, W. 1984, Handbook of Applicable Mathematics. Volume 6A–B: Statistics (Wiley–Blackwell)
 Liu, L., Gerke, B. F., Wechsler, R. H., Behroozi, P. S., & Busha, M. T. 2011, ApJ, 733, 62
 LSST Dark Energy Science Collaboration. 2012, arXiv e-prints, arXiv:1211.0310
 LSST Dark Energy Science Collaboration (LSST DESC), Abolfathi, B., Alonso, D., et al. 2021, ApJS, 253, 31
 LSST Science Collaboration, Abell, P. A., Allison, J., et al. 2009, arXiv e-prints, arXiv:0912.0201
 Mandelbaum, R., Seljak, U., Cool, R. J., et al. 2006, MNRAS, 372, 758
 More, S., van den Bosch, F. C., Cacciato, M., et al. 2009, MNRAS, 392, 801
 Moster, B. P., Naab, T., & White, S. D. M. 2018, MNRAS, 477, 1822
 Neistein, E., Weinmann, S. M., Li, C., & Boylan-Kolchin, M. 2011, Monthly Notices of the Royal Astronomical Society, 414, 1405
 Payerne, C., Zhang, Z., Aguena, M., et al. 2025, arXiv e-prints, arXiv:2502.08444
 Peacock, J. A. & Smith, R. E. 2000, MNRAS, 318, 1144
 Phillipps, S. & Shanks, T. 1987, MNRAS, 229, 621
 Rodriguez, F. & Merchán, M. 2020, A&A, 636, A61
 Rodriguez, F., Merchán, M., & Sgró, M. A. 2015, A&A, 580, A86
 Rykoff, E. S., Rozo, E., Busha, M. T., et al. 2014, ApJ, 785, 104
 Schmidt, S. J., Malz, A. I., Soo, J. Y. H., et al. 2020, MNRAS, 499, 1587
 Soccimarro, R., Sheth, R. K., Hui, L., & Jain, B. 2001, ApJ, 546, 20
 Seljak, U. 2000, MNRAS, 318, 203
 Spergel, D., Gehrels, N., Baltay, C., et al. 2015, arXiv e-prints, arXiv:1503.03757
 Springel, V., White, S. D. M., Jenkins, A., et al. 2005, Nature, 435, 629
 Tempel, E., Einasto, J., Einasto, M., Saar, E., & Tago, E. 2009, A&A, 495, 37
 Tinker, J. L., Weinberg, D. H., Zheng, Z., & Zehavi, I. 2005, ApJ, 631, 41
 van den Bosch, F. C., Yang, X., & Mo, H. J. 2003, MNRAS, 340, 771
 van den Bosch, F. C., Yang, X., Mo, H. J., et al. 2007, MNRAS, 376, 841

- Van Kampen, W., Cluver, M. E., Taylor, E. N., et al. 2025, arXiv e-prints, arXiv:2508.12556
- Wechsler, R. H., Somerville, R. S., Bullock, J. S., et al. 2001, ApJ, 554, 85
- White, M., Zheng, Z., Brown, M. J. I., Dey, A., & Jannuzi, B. T. 2007, ApJ, 655, L69
- White, S. D. & Rees, M. J. 1978, Monthly Notices of the Royal Astronomical Society, 183, 341
- Yang, X., Mo, H., Van Den Bosch, F. C., & Jing, Y. 2005, Monthly Notices of the Royal Astronomical Society, 356, 1293
- Yang, X., Mo, H. J., & van den Bosch, F. C. 2008, ApJ, 676, 248
- Yang, X., Xu, H., He, M., et al. 2021, ApJ, 909, 143
- Zandivarez, A., Díaz-Giménez, E., Taverna, A., Rodríguez, F., & Merchán, M. 2024, A&A, 691, A6
- Zheng, Z., Berlind, A. A., Weinberg, D. H., et al. 2005, ApJ, 633, 791
- Zou, H., Gao, J., Xu, X., et al. 2021, ApJS, 253, 56

Appendix A: CGF

We explore the impact of varying the free parameters (f_r, f_z) in the CGF method. Fig. A.1 shows the median *purity* (top) and *completeness* (bottom) of the CGF as a function of halo mass (M_{200}) over the range 10^{12} – $10^{15} M_\odot$. The values in each cell of the table correspond to various combinations of the CGF parameters f_r and f_z , which control the projected and redshift-space exclusion regions during iterative centre selection.

As discussed in the main text, a clear trade-off emerges: higher values of f_r and f_z increase the exclusion volume, improving the *purity*—defined as the fraction of selected central candidates that are truly centrals—while reducing *completeness*, the fraction of true centrals correctly identified. In contrast, lower parameter values yield better *completeness* at the expense of *purity*, as more contaminants are retained.

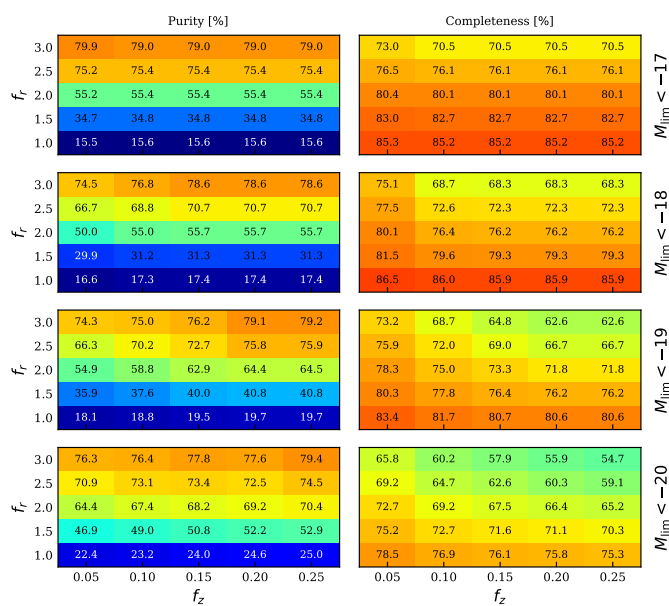


Fig. A.1. Mean *purity* (left panel) and *completeness* (right panel) of the CGF, obtained by averaging these quantities over haloes with masses in the range 10^{12} – $10^{15} M_\odot$. Each panel corresponds to a different combination of the CGF parameters f_r and f_z . Increasing f_r and f_z leads to higher mean *purity* but lower mean *completeness*, while smaller values improve *completeness* at the cost of greater contamination.

These results illustrate the motivation behind our adopted parameter choice of $(f_r, f_z) = (2.5, 0.25)$, which maintains *purity* above $\sim 70\%$ while preserving acceptable *completeness*, especially important in the context of large upcoming photometric surveys such as LSST. This combination of parameters also yields a distribution of identified groups that is broadly consistent with those found using the original group sample, as shown in Fig. A.2. For this comparison, we compute the Kolmogorov–Smirnov (KS, Lederer 1984) statistic (D^{KS}) over the full dataset to quantify the maximum deviation between the CGF-identified group centres and those in the original sample. The resulting p -values ($p \gg 0.05$) indicate no significant difference between the two distributions, supporting the accuracy of the CGF in recovering the underlying group-centre distribution. However, it is important to note that this comes at the

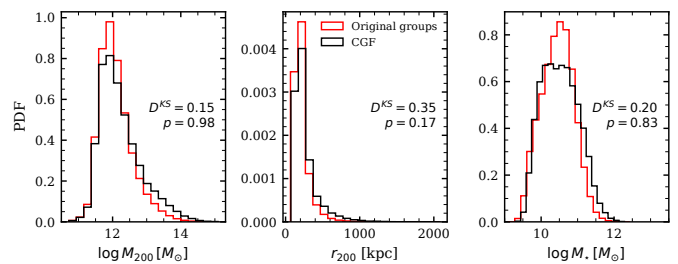


Fig. A.2. Normalized distributions of halo mass M_{200} (left panel), halo radius r_{200} (middle panel), and stellar mass M_\star (right panel) of CGF vs. the original groups sample. KS statistics and p -values for each comparison are shown in the panels.

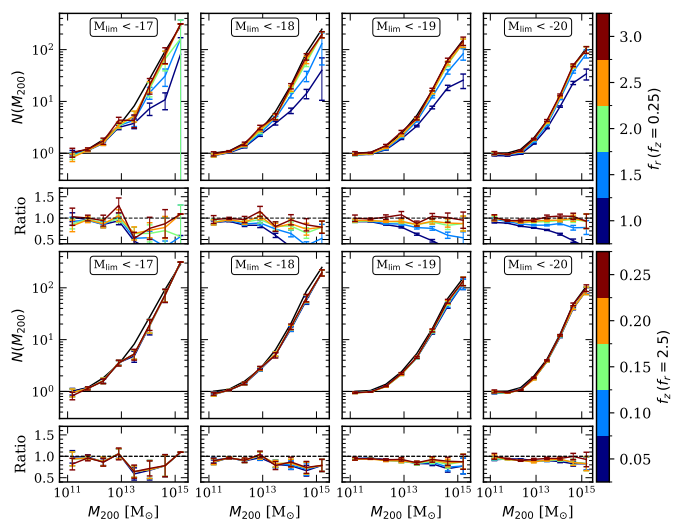


Fig. A.3. (Top panels) BST results using a fixed redshift parameter $f_z = 0.25$ and varying f_r parameter. (Bottom panels) Results using a fixed $f_r = 2.5$ and varying the redshift parameter f_z . The performance shows better agreement with the true HOD as f_r increases, while it does not change significantly when varying f_z .

cost of a substantial reduction in the number of groups included in the CGF sample, reflecting the trade-off between *purity* and *completeness* of the CGF method.

To further evaluate the impact of the CGF parameters on the accuracy of central galaxy identification, we conduct the BST varying one parameter at a time while fixing the other to a representative pivot value ($f_r = 2.5$ or $f_z = 0.25$). The results, shown in Fig. A.3, highlight how greater discard radii (specifically $r_{\text{dsc}} < 2.5 r_c^{\text{lum}}$) lead to better agreement with the HOD. This improvement is directly related to the resulting *purity* of the CGF, which is essential to faithfully recover the underlying HOD signal.

Only for $f_r = 2.5$ and $f_r = 3.5$, where the *purity* exceeds roughly 70% , we obtain good agreement with the true HOD. This is particularly important in the high-mass regime, where the HOD is more sensitive to contamination. This analysis supports our choice of parameters for the main catalogue used in the following sections.

Appendix B: Inference of the halo mass

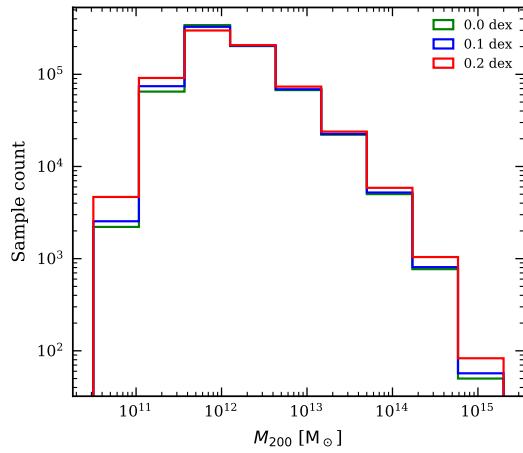


Fig. B.1. Distribution of halo masses in the group sample. The green curve shows the original distribution, while the blue and red curves represent the perturbed distributions obtained by adding Gaussian scatter in M_{200} with different standard deviations (in dex).

To assess the impact of halo mass uncertainties on the overall distribution, we introduce Gaussian perturbations with varying standard deviations (in dex) to the original M_{200} values. As shown in Fig. B.1, increasing the level of scatter leads to a broader redistribution of halo masses. Notably, this results in a net increase in the number of haloes at both the low- and high-mass ends, as objects are scattered into the tails of the distribution from the central mass range.